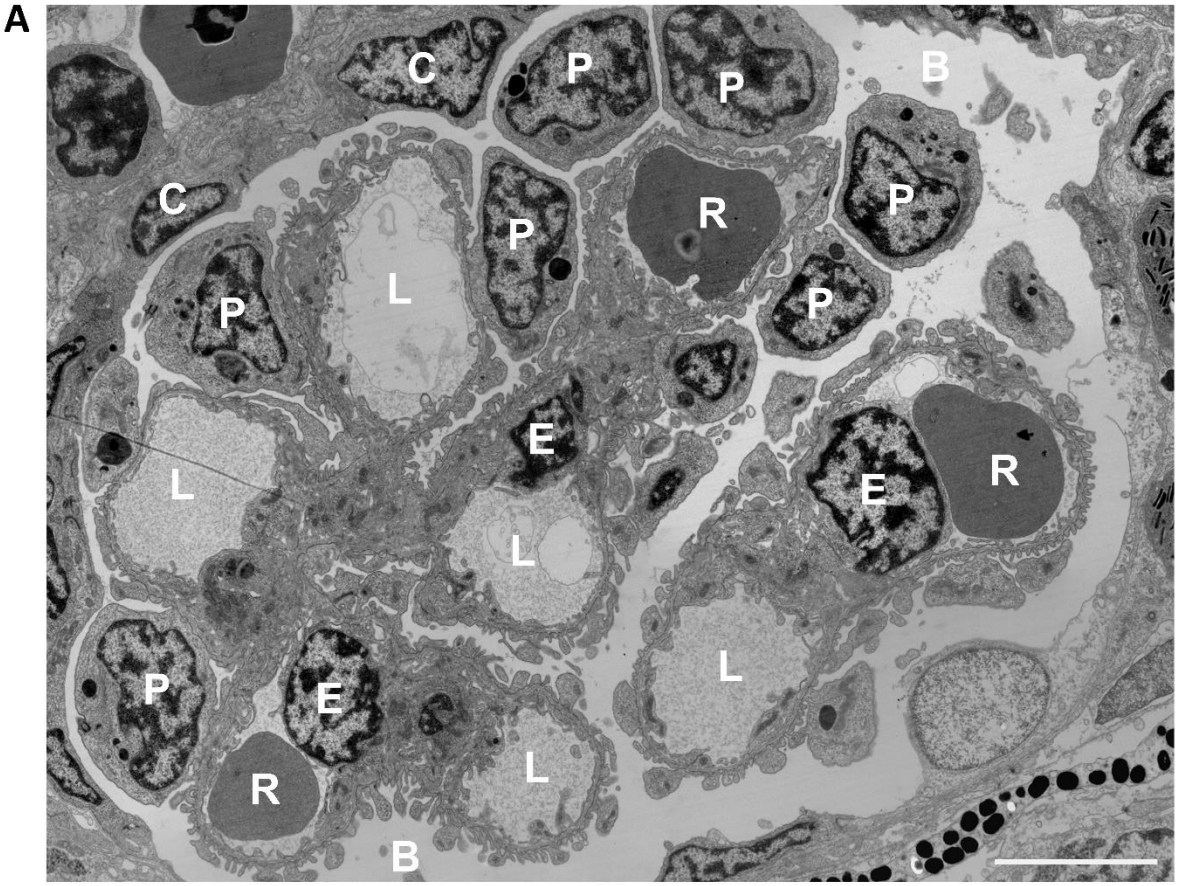

Suppl. Figure 1. Representative overview over the glomerular histology in adult zebrafish via electron microscopy.
(A) Stitched together overview of a full glomerulus in an adult zebrafish kidney visualized via electron microscopy. The zebrafish glomerulus shows the common architecture encountered in vertebrate animals: Central to the glomerulus is a tuft of tangled capillaries with many capillary lumen (L) visualized in cross-section here. Several lumen show erythrocytes (R) inside in close relation to the endothelial nuclei (E) visible in some capillaries. This vascular tuft is surrounded by a layer of specialized epithelial cells, namely the podocytes (P), which share the glomerular basement membrane with the endothelial cells and thereby form the filtration barrier. The ultrafiltrate is pressed from there into the bowman's space (B), which is encapsulated by the bowman's capsule (C). The white scale bar is 5 µm.

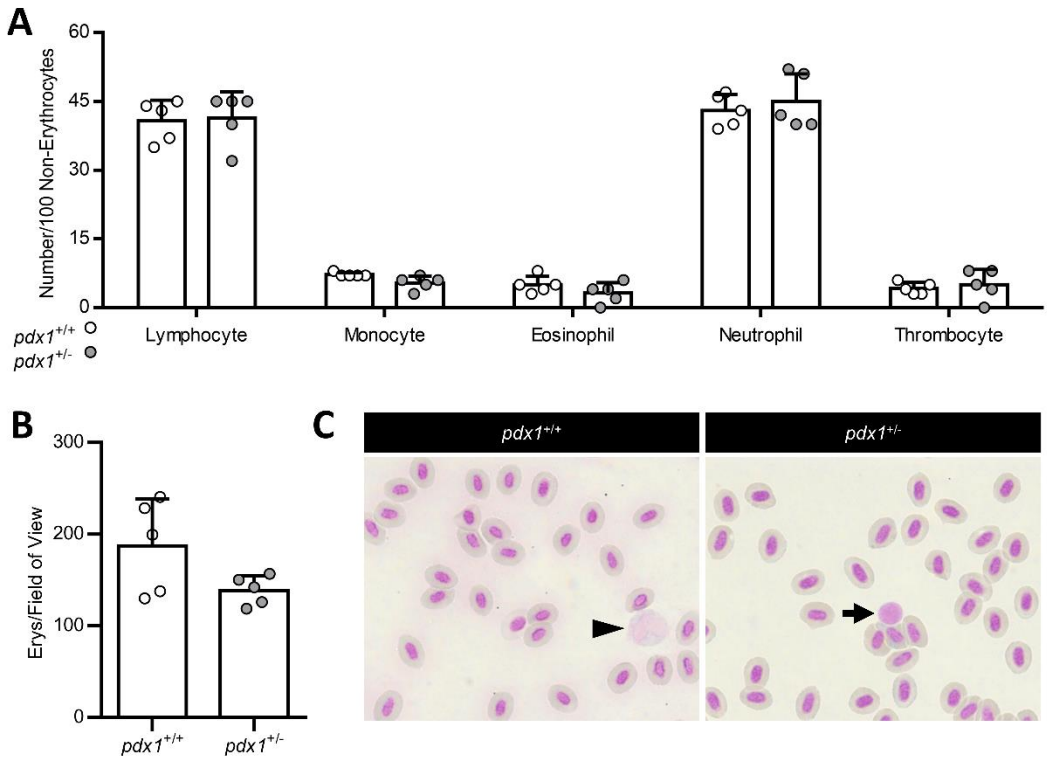

Suppl. Figure 2. Peripheral blood smear shows no alterations in the blood cell constitution of adult *pdx1*$^{+/-}$ mutants
(A) Non-erythrocyte blood cell content in peripheral blood smears from adult *pdx1*$^{+/+}$ (n = 5) and *pdx1*$^{+/-}$ (n = 5) zebrafish. Per sample 100 non-erythrocytes were analyzed microscopically after May-Grünwald staining. It is important to note that in comparison to humans, in zebrafish only two distinct forms of granulocytes, neutrophils/heterophils and eosinophils, have been described. **(B)** Erythrocyte cell count per ten fields of view (FOV) at 63x magnification in adult *pdx1*$^{+/+}$ (n =5) and *pdx1*$^{+/-}$ (n =5) zebrafish. Peripheral blood smear was performed with May-Grünwald stain. **(C)** Representative light microscopy of peripheral blood smear after May-Grünwald stain in adult *pdx1*$^{+/+}$ and *pdx1*$^{+/-}$ zebrafish. Erythrocytes are nucleated cells in zebrafish and make up most of the blood content. A singular neutrophil (black arrowhead) and lymphocyte (black arrow) are marked on the images exemplary. Statistics utilized two-way ANOVA + Sidak's multiple comparison test in (A) and t-test in (B); mean + SD.

A

KEGG Pathway	Main Category	Sub Category	NES	Adj. P-Value
dre01100_Metabolic_pathways	1. Metabolism	1.0 Global and overview maps	-1.23	0.0229
dre00020_Citrate_cycle_(TCA_cycle)	1. Metabolism	1.1. Carbohydrate metabolism	-1.82	0.0127
dre00564_Glycerophospholipid_metabolism	1. Metabolism	1.3. Lipid metabolism	-1.54	0.0348
dre00270_Cysteine_and_methionine_metabolism	1. Metabolism	1.5. Amino acid metabolism	-1.7	0.0182
dre00860_Porphyrin_and_chlorophyll_metabolism	1. Metabolism	1.8. Metabolism of cofactors and vitamins	-1.68	0.0366
dre00760_Nicotinate_and_nicotinamide_metabolism	1. Metabolism	1.8. Metabolism of cofactors and vitamins	-1.59	0.0476
dre03022_Basal_transcription_factors	2. Genetic Information Processing	2.1. Transcription	-1.66	0.0341
dre00970_Aminoacyl-tRNA_biosynthesis	2. Genetic Information Processing	2.2. Translation	-2.06	0.0052
dre03015_mRNA_surveillance_pathway	2. Genetic Information Processing	2.2. Translation	-1.65	0.014
dre03013_RNA_transport	2. Genetic Information Processing	2.2. Translation	-1.49	0.0275
dre03050_Proteasome	2. Genetic Information Processing	2.3. Folding, sorting and degradation	2.58	0.0052
dre03018_RNA_degradation	2. Genetic Information Processing	2.3. Folding, sorting and degradation	-1.71	0.0098
dre04120_Ubiquitin_mediated_proteolysis	2. Genetic Information Processing	2.3. Folding, sorting and degradation	-1.6	0.0098
dre04330_Notch_signaling_pathway	3. Environmental Information Processing	3.2. Signal transduction	-1.53	0.0467
dre04010_MAPK_signaling_pathway	3. Environmental Information Processing	3.2. Signal transduction	-1.68	0.0052
dre04012_ErbB_signaling_pathway	3. Environmental Information Processing	3.2. Signal transduction	-1.72	0.0052
dre04068_FoxO_signaling_pathway	3. Environmental Information Processing	3.2. Signal transduction	-1.72	0.0052
dre04070_Phosphatidylinositol_signaling_system	3. Environmental Information Processing	3.2. Signal transduction	-1.64	0.0098
dre04150_mTOR_signaling_pathway	3. Environmental Information Processing	3.2. Signal transduction	-1.56	0.0098
dre04310_Wnt_signaling_pathway	3. Environmental Information Processing	3.2. Signal transduction	-1.47	0.0245
dre04060_Cytokine-cytokine_receptor_interaction	3. Environmental Information Processing	3.3. Signaling molecules and interaction	1.45	0.0275
dre04514_Cell_adhesion_molecules_(CAMs)	3. Environmental Information Processing	3.3. Signaling molecules and interaction	1.45	0.0366
dre04144_Endocytosis	4. Cellular Processes	4.1. Transport and catabolism	-1.54	0.0052
dre04140_Autophagy	4. Cellular Processes	4.1. Transport and catabolism	-1.43	0.0457
dre04210_Apoptosis	4. Cellular Processes	4.2. Cell growth and death	-1.5	0.0214
dre04110_Cell_cycle	4. Cellular Processes	4.2. Cell growth and death	-1.5	0.0307
dre04114_Oocyte_meiosis	4. Cellular Processes	4.2. Cell growth and death	-1.67	0.0052
dre04218_Cellular_senescence	4. Cellular Processes	4.2. Cell growth and death	-1.8	0.0052
dre04216_Ferroptosis	4. Cellular Processes	4.2. Cell growth and death	-1.74	0.0098
dre04510_Focal_adhesion	4. Cellular Processes	4.3. Cellular community - eukaryotes	-1.52	0.0098
dre04540_Gap_junction	4. Cellular Processes	4.3. Cellular community - eukaryotes	-1.57	0.0187
dre04520_Adherens_junction	4. Cellular Processes	4.3. Cellular community - eukaryotes	-1.49	0.0492
dre04810_Regulation_of_actin_cytoskeleton	4. Cellular Processes	4.5. Cell motility	-1.69	0.0052
dre04910_Insulin_signaling_pathway	5. Organismal Systems	5.2. Endocrine system	-1.66	0.0052
dre04912_GnRH_signaling_pathway	5. Organismal Systems	5.2. Endocrine system	-1.72	0.0052
dre04914_Progesterone-mediated_oocyte_maturation	5. Organismal Systems	5.2. Endocrine system	-1.7	0.0096
dre04270_Vascular_smooth_muscle_contraction	5. Organismal Systems	5.3. Circulatory system	-1.72	0.0052
dre05132_Salmonella_infection	6. Human Diseases	6.8. Infectious diseases: Bacterial	-1.5	0.0457

Suppl. Figure 3. Multiple pathways associated with the development of a diabetic metabolism are differentially regulated in the adult heterozygous *pdx1*$^{+/-}$ zebrafish kidney.

(A) Full list of differentially regulated KEGG pathways of RNA-seq data from adult heterozygous *pdx1*$^{+/-}$ kidney tissue (n = 9) compared to tissue from wildtype clutch mates (n = 3) with multiple targets being associated with the development of a diabetic metabolism. For each KEGG pathway, the main and sub category, as well as normalized enrichment scores (NES) and adjusted p-values are reported.

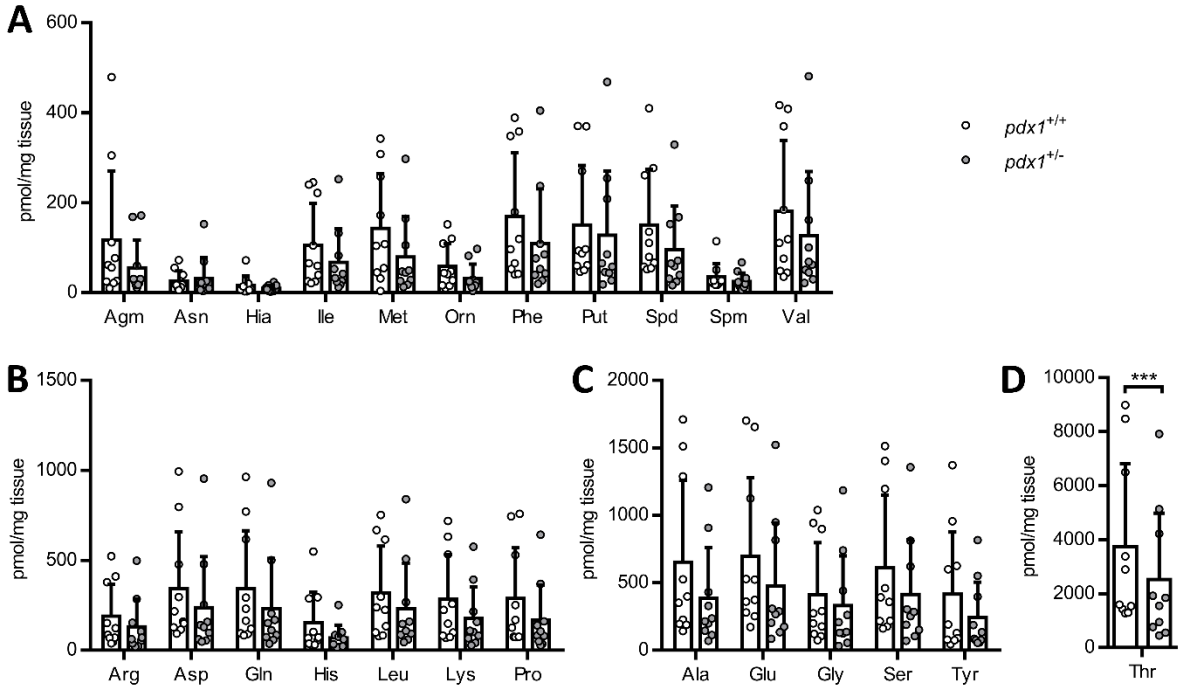

Suppl. Figure 4. Free amino acid levels are lowered in kidney tissue from heterozygous *pdx1*$^{+/-}$ zebrafish mutants.
(A-D) Metabolome analysis uncovered overall lowered free amino acid levels in heterozygous *pdx1*$^{+/-}$ zebrafish kidney tissue (n = 10) compared to wildtypes (n = 10). Results below background levels were excluded. Data is visualized in four distinct concentration groups: low (A), middle (B), high (C), abundant (D). Two-way ANOVA proved both significant main effects for zebrafish genotype ($p^{*} = 0{,}0189$) and amino acid type ($p^{****} < 0{,}0001$), but no significant interaction between both groups ($p = 0{,}8063$). The post-hoc test revealed a significant reduction of threonine amount in the heterozygous *pdx1*$^{+/-}$ kidney tissue. Statistics utilized two-way ANOVA + Sidak's multiple comparison test including all groups (A-D); mean + SD; $^{***}p < 0{,}001$. Symbol legend: Agm = Agmatine; Ala = Alanine; Arg = Arginine; Asn = Asparagine; Asp = Aspartate; Gln = Glutamine; Glu = Glutamate; Gly = Glycine; Hia = Histamine; His = Histidine; Ile = Isoleucine; Leu = Leucine; Lys = Lysine; Met = Methionine; Orn = Ornithine; Phe = Phenylalanine; Pro = Proline; Put = Putrescine; Ser = Serine; Spd = Spermidin; Spm = Spermin; Thr = Threonine; Tyr = Tyrosine; Val = Valine.

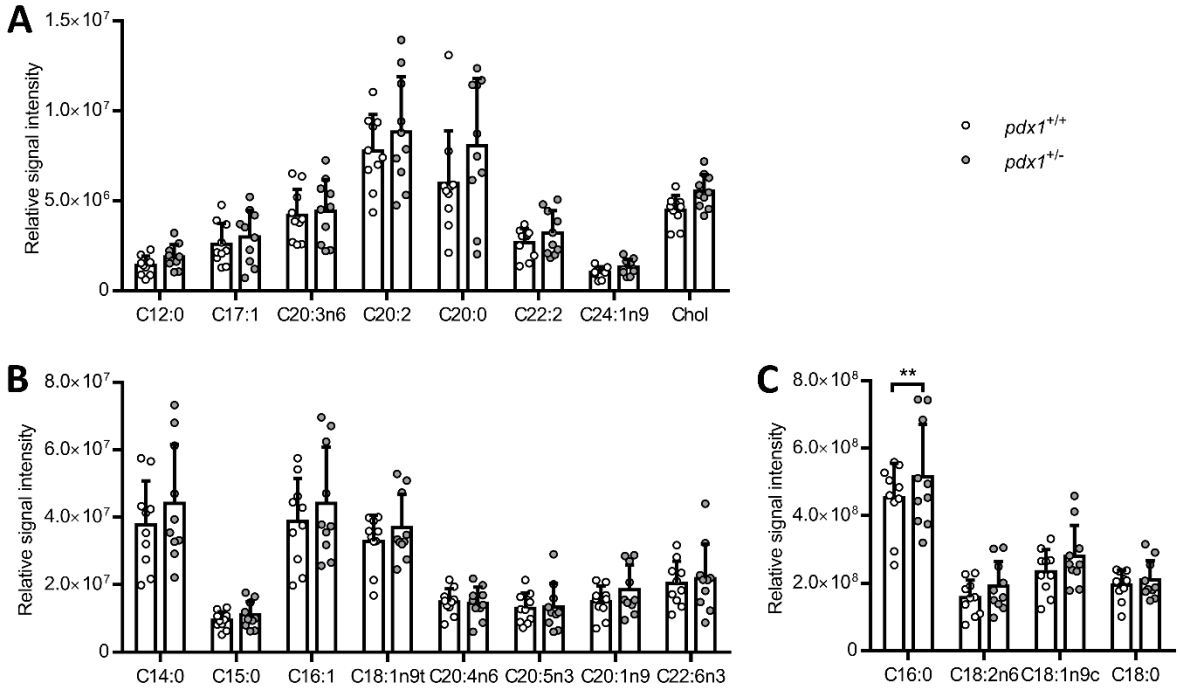

Suppl. Figure 5. Free fatty acid acid levels are increased in kidney tissue from heterozygous *pdx1*$^{+/-}$ zebrafish mutants.
(A-D) Metabolome analysis uncovered overall increased free fatty acid levels in heterozygous *pdx1*$^{+/-}$ zebrafish kidney tissue (n = 10) compared to wildtypes (n = 10). Results below background levels were excluded. Data is visualized in three distinct signal intensity groups relative to an internal standard: low (A), middle (B), high (C). Two-way ANOVA proved both significant main effects for zebrafish genotype (p* = 0,0189) and fatty acid type (p**** = <0,0001), but no significant interaction between both groups (p = 0,4834). The post-hoc test revealed a significant increase of palmitic acid (C16:0) amount in the heterozygous *pdx1*$^{+/-}$ kidney tissue. Statistics utilized two-way ANOVA + Sidak's multiple comparison test including all groups (A-C); mean + SD; **p < 0,01.

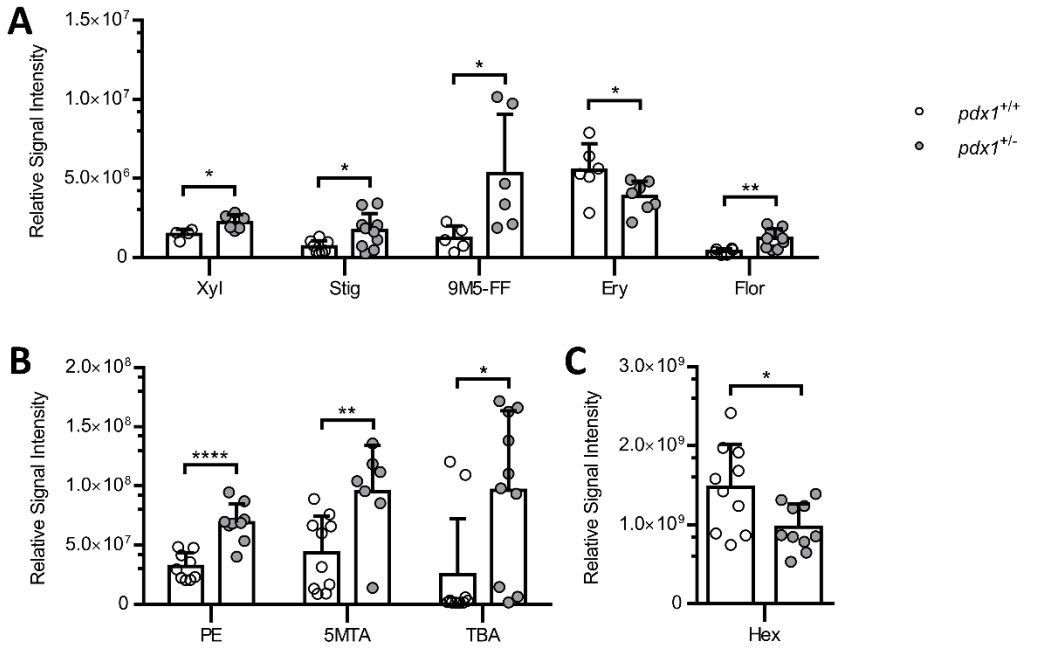

Suppl. Figure 6. Adult heterozygous *pdx1*$^{+/-}$ zebrafish show several metabolic alterations in their primary metabolites
(A-C) Significant GCMS results of different relative amounts of primary metabolites in adult heterozygous *pdx1*$^{+/-}$ zebrafish kidney tissue (n = 10) compared to wildtypes (n = 10). Results below background levels were excluded. Data is visualized in three distinct signal intensity groups relative to an internal standard: low (A), middle (B), high (C). Statistics utilised multiple t-test; mean + SD; *p < 0,05; **p < 0,01; ***p < 0,001. Symbol legend: Xyl = Xylitol; Stig = Stigmasterol; 9M5-FF = 9-(3-methyl-5-pentylfuran-2-yl)nonanoate; Ery = Erythrono-1,4-lactone; Flor = 2-O-Glycerol-a-d-galactopyranoside (Floridoside); PE = Phosphoethanolamine; 5MTA = 5'-Methylthioadenosine; TBA = 2,3,4-Trihydroxybutyricacid; Hex = Representing hexoses like glucose/mannose/galactose.

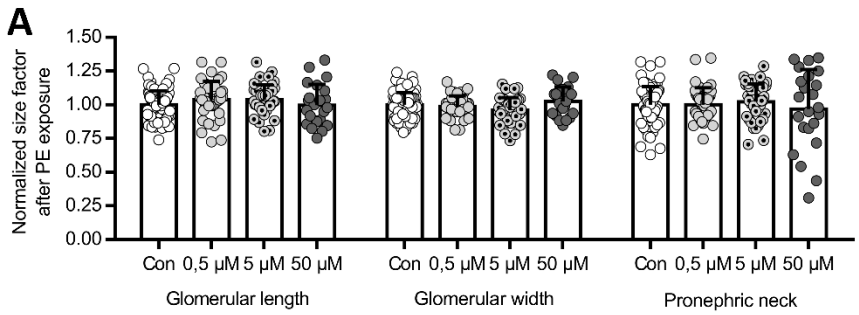

Suppl. Figure 7. Phosphoethanolamine induces no morphological alterations in the pronephros at 48 hpf.
(A) Concentrations of up to 50 µM phosphoethanolamine (PE) show no influence on the pronephric phenotype in wildtype *Tg(wt1b:EGFP)* zebrafish embryos at 48 hpf (n = 80 for control with DMSO, n = 39 for 0,5 µM, n = 42 for 5 µM and n =23 for 50 µM). Measurements were normalized to the respective control mean to allow for interexperimental comparison. Statistics utilized two-way ANOVA + Sidak's multiple comparison test; mean + SD.

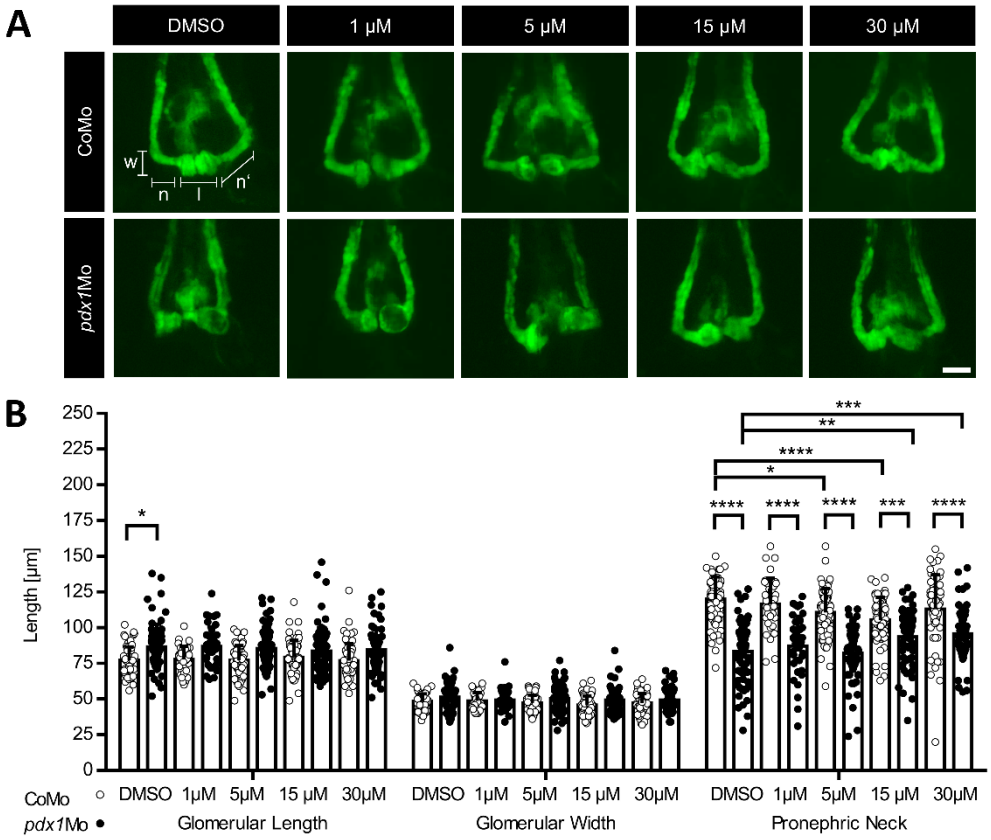

Suppl. Figure 8. Meclizine treatment partially rescues morphological alterations induced via *pdx1* knockdown in the pronephros at 48 hpf.

(A) Representative visualization of the morphological fluorescent pronephros phenotype after *pdx1* morpholino (*pdx1*Mo) and control morpholino (CoMo) injection in *Tg(wt1b:EGFP)* embryos with additional co-incubation with Meclizine at different concentrations until 48 hpf. **(B)** Evaluation of a Meclizine treatment to rescue *pdx1*Mo-induced pronephros alterations in *Tg(wt1b:EGFP)* zebrafish embryos at 48 hpf. 15µM and 30µM Meclizine treatment partially rescued the pronephric neck length shortening in *pdx1* morpholino injected embryos (for *pdx1*Mo: n = 68 for DMSO, n = 38 for 1 µM, n = 67 for 5 µM, n = 67 for 15 µM, n = 67 for 30 µM). Meclizine itself induced slight neck length shortening in the CoMo-injected group in the range of 5µM and 15µM, all the while rescuing the *pdx1* morpholino-mediated effect, making it likely that these effects are mediated through different mechanisms (for CoMo: n = 67 for DMSO, n = 37 for 1 µM, n = 67 for 5 µM, n = 66 for 15 µM, n = 64 for 30 µM). The pronephric dimensions have been marked exemplary in (A). Glomerular width represents a single measurement (w), while data points for pronephric neck length (n+n') and glomerular length (l) represent measurements for both the left and right pronephric side added up. The white scale bar is 50 µm in (A). Statistics utilized two-way ANOVA + Turkey's multiple comparison test; mean + SD; *p < 0,05; **p < 0,01; ***p < 0,001; ****p < 0,0001.

Suppl. Methods 1. Additional information regarding the glomerular hypertrophy and nuclei analysis.
Kidney tissue from n = 4 fish per group was sectioned longitudinally to provide a complete overview over the head, trunk and tail region of the kidney. Two consecutive sections were selected, and all glomeruli were identified in both sections. Only glomeruli, which were identified in both sections were chosen for further analysis to avoid including glomerular data from the edge of the glomerulus. From this subset, 10 glomeruli per sample were randomly chosen and for each glomerulus the larger glomerular cut from the two consecutive sections was selected for inclusion into the analysis. Glomerular area was quantified via the ImageJ freehand tool and nuclei were manually counted.

Suppl. Methods 2. Additional information regarding the metabolite determination via GC/MS.

Sample extraction: Frozen sample material was extracted with 190 µL 100% methanol containing 10 µL 0.02 mg/ml Ribitol for 15 min. at 70°C with vigorous shaking. After the addition of 100 µL 100% chloroform containing 20 mg/mL Heptadecanoic acid (C17:0), samples were shaken at 37°C for 5 min. To separate polar and organic phases, 200 µL HPLC-grade water were added and samples were centrifuged for 10 min at 11,000x g. while avoiding the interphase containing cellular debris, 350 µL of the polar (upper) phase were transferred to a fresh glass vial and dried using a vacuum concentrator (Eppendorf Concentrator Plus) without heating. To analyze total fatty acids, 75µl of the lower organic phase (chloroform) after extraction were transferred to a fresh glass vial and dried in a vacuum concentrator without heating.

Derivatization for Metabolite Analysis (Methoximation and Silylation): Sequential on-line methoximation and silylation reactions were performed using a MPS autosampler (Gerstel, Mülheim Ruhr). Methoximation was performed by adding 20 µL 20 mg/ml methoxyamine hydrochloride (Sigma 226904) in pyridine (Sigma 270970) and incubation at 37°C for 90 min in an Gerstel MPS Agitator Unit (250 rpm). For silylation reactions, 45 µl of N-Methyl-N-(trimethylsilyl)trifluoroacetamide (MSTFA; Sigma 69479) were added and samples were incubated at 37°C for 30 min with gentle shaking. Before injection, samples were incubated at RT for 45 min.

Gas Chromatography/Mass Spectrometry (GC/MS) analysis for metabolites: For GC/MS analysis, a GC-ToF system was used consisting of an Agilent 7890 Gas Chromatograph (Agilent, Santa Clara) fitted with a Rxi-5Sil MS column (30 meter x 0.25 mm x 0.25 µm; Restek Corporation, Bellefonte) coupled to a Pegasus BT Mass Spectrometer (LECO Corporation, Michigan). The GC was operated with an injection temperature of 250°C and 1 µL sample was injected in splitless mode. The GC temperature program started with a 1 min. hold at 40°C followed by a 6°C/min ramp up to 210°C, a 20°C/min ramp up to 330°C and a bake-out at 330°C for 5 min. using Helium as carrier gas with constant linear velocity. The ToF mass spectrometer was operated with ion source and interface temperatures of 250°C, a solvent cut time of 9 min and a scan range (m/z) of 50 – 600 with an acquisition rate of 17 spectra/second. The ChromaTof v5.50 software (LECO Corporation, Michigan) was used for data processing.

Derivatization for Total Fatty Acid Analysis: Sequential on-line transmethylation reactions were performed using a MPS autosampler (Gerstel, Mülheim Ruhr). First, pellets were re-dissolved for 5 min at 50°C at 500 rpm in 40µL TBME (tert-Butyl methyl ether, Sigma) and 20µL TMSH (Trimethylsulfoniumhydroxid, Sigma), incubated for 45 min. at 50°C and 500 rpm.

Gas Chromatography/Mass Spectrometry (GC/MS) analysis for Total Fatty Acid Analysis: A GC/MS-QP2010 Plus (Shimadzu®) fitted with a Zebron ZB 5MS column (Phenomenex®; 30 meter x 0.25 mm x 0.25 µm) was used for GC/MS analysis. The GC was operated with an injection temperature of 230°C and 1µL sample was injected with splitless mode. The GC temperature program started with a 1 min. hold at 40°C followed by a 6°C/min ramp to 210°C, a 20°C/min ramp to 330°C and a bake-out for 5 min. at 330°C using Helium as carrier gas with constant linear velocity. The MS was operated with ion source and interface temperatures of 250°C, a solvent cut time of 7 min and a scan range (m/z) of 40–700 with an event time of 0.2 sec. The "GCMS solution" software (Shimadzu®) was used for data processing.